Review of “Assessing Cloud Representation in Two Microphysics Schemes of MPAS- Atmosphere Model (version 8.2.2) over the Maritime Continent with Himawari-9 AHI Observations”

Recommendation:

Major revisions:

General comments:

This manuscript evaluates cloud characteristics simulated by MPAS with two cloud microphysics schemes using observations from the Himawari-9 Advanced Himawari Imager (AHI). The two schemes examined are the single-moment bulk microphysics scheme WSM6 and the two-moment NSSL scheme. The authors performed a set of twelve 48-hour simulations with different initialization dates over the Maritime Continent, centered near Singapore. The satellite radiative transfer model RTTOV was applied to the MPAS output to simulate brightness temperatures, which were then compared with Himawari-9 AHI observations in ten spectral channels of infrared radiation. Based on these comparisons, the authors attempt to identify and characterize the differences between the two microphysics schemes.

The methodology adopted in this study using satellite simulators has become relatively common in recent years. The distinctive aspect of this paper is the comprehensive use of all ten AHI infrared channels. Since the different channels are sensitive to different cloud microphysical and macrophysical properties, they provide valuable information for evaluating model performance.

The authors tried to describe various aspects of the difference between the results from the two schemes. The manuscript presents results from many channels and discusses specific aspects of cloud characteristics. However, it is difficult to understand the characteristics of the two schemes in terms of the physical space. Cross sections of cloud microphysics are not so informative, because their generality is unclear. The reviewer suggests some alternative analysis below to show more robustness of the differences. If the manuscript is substantially revised to improve the clarity and consistency of the analysis, I believe it could be suitable for publication in *Geoscientific Model Development (GMD)*.

1) First, the reviewer requests a comparison of the horizontal distributions of brightness temperatures in selected AHI channels between the observations and the two model simulations. Instead, the authors attempt to draw general conclusions primarily from a few sample cross sections (e.g., Fig. 2). Horizontal maps would more clearly illustrate the differences in cloud coverage and spatial cloud structures between the observations and the two microphysics schemes.

Reply: We thank the reviewer for this helpful suggestion. We have expanded the analysis from individual cross sections to a broader horizontal evaluation by examining the mean distributions of AHI channel-13 forecast-minus-observation (F−O) brightness-temperature differences accumulated over multiple verification times for both the WSM6 and NSSL simulations, allowing more general conclusions to be drawn. These horizontal distributions provide a direct measure of the spatial differences between the simulated and observed infrared cloud signatures. For the cloud-sensitive infrared window channel 13, positive F–O values in cloud-dominated regions indicate warmer simulated BTs than observed, generally associated with insufficient high/cold-cloud coverage, lower cloud tops, and/or optically thinner clouds. Negative F − O values indicate colder simulated BTs and are generally associated with excessive high/cold-cloud coverage, higher cloud tops, and/or optically thicker clouds.

As shown in Figures 3a–b, WSM6 exhibits more widespread positive F–O differences, indicating a systematic warm bias in the simulated channel-13 BTs. In contrast, NSSL shows smaller F–O biases overall, particularly over 5−10°N, although localized cold biases remain. This spatial behavior is broadly consistent with the channel-13 BT frequency distributions in Figure 2, where NSSL more closely reproduces the observed occurrence of BTs below ~230 K. Together, these results suggest that NSSL provides a more realistic representation of cold-cloud characteristics than WSM6.

To further investigate the physical origin of these observation-space differences and relate them to model-space cloud properties, we additionally examined the horizontal distributions of channel-13 F–O BT differences together with simulated outgoing longwave radiation (OLR) and cloud ice water path (CIWP), as discussed in detail in our response to Comment 2).

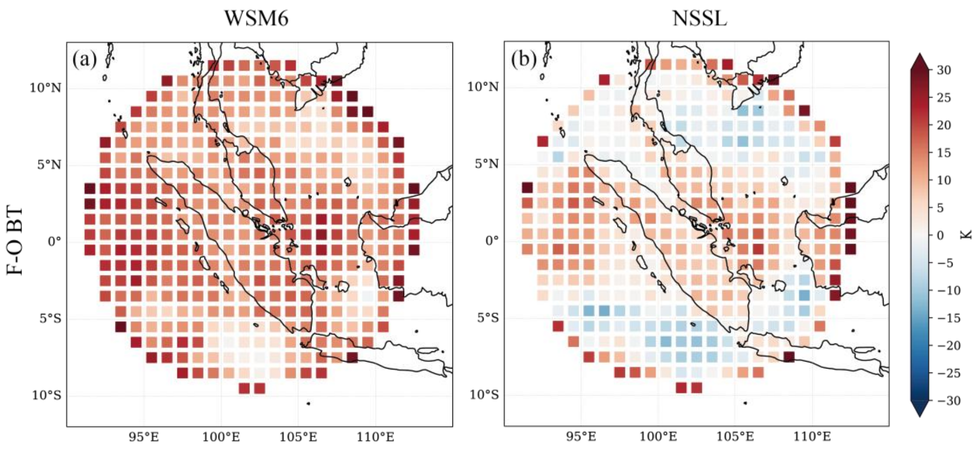

Figure 3. Daily-mean horizontal distributions of AHI channel-13 forecast-minus-observation (F–O) brightness-temperature differences for (a) WSM6 and (b) NSSL. Statistics are computed from 24–48 h forecasts at 6 h intervals using cloudy samples.

2) Second, the reviewer suggests that the authors should compare physical variables between the observations and the models. The cloud characteristics of the models are generally evaluated by daily mean horizontal distributions of outgoing longwave radiation (OLR) and outgoing shortwave radiation (OSR) by comparing the CERES observations. For the cloud distribution, the ISCCP diagram analysis is the standard method of model evaluation. How these physical-space analyses can be used to interpret the AHI-based analysis presented in this study is an interesting question. In addition, the domain-averaged vertical distributions of cloud hydrometeors (Fig. 8) help illustrate differences among the models. However, it is not clear how these differences in the vertical cloud profiles are consistent with the results shown in Figs. 5 and 6. Please clarify the relationship between these diagnostics.

Reply: Thank you for this valuable suggestion.

1) We agree that physical-space diagnostics are useful for interpreting radiance-space differences and for clarifying how the simulated cloud structures differ between the two microphysics schemes.The primary objective of this study is to assess cloud representation from the perspective of thermal-infrared AHI radiances and to examine its sensitivity to microphysics. We therefore focus on OLR, which is more directly related to the longwave emission sampled by AHI channel 13, together with CIWP as a model-space measure of ice-cloud amount. These diagnostics are used to provide a physical-space interpretation of the AHI-based evaluation. In the revised manuscript, we therefore added daily-mean horizontal distributions of simulated outgoing longwave radiation (OLR) and cloud ice water path (CIWP), together with the AHI channel-13 F – O brightness-temperature differences (new Figure 3)

The added analysis shows a physically consistent relationship among these diagnostics. WSM6 exhibits widespread positive channel-13 F−O differences, indicating systematically warmer simulated BTs than observed. These regions generally coincide with higher OLR and lower CIWP, suggesting less abundant upper-level ice clouds. In contrast, NSSL shows smaller F–O biases, particularly in the northern part of the analysis region, where lower OLR and substantially larger CIWP indicate a greater amount of upper-level ice cloud. This spatial relationship is also consistent with the channel-13 BT frequency distributions in Fig. 2, where NSSL more closely reproduces the observed occurrence of cold BTs below approximately 230 K. The domain-averaged vertical hydrometeor profiles in Fig. 8 provide further physical support by showing differences in upper-level frozen hydrometeor content between the two schemes. Thus, the horizontal OLR and CIWP distributions provide a direct physical-space interpretation of the channel -13 BT differences, while the vertical hydrometeor profiles help explain the underlying cloud-structure differences responsible for these contrasting radiative signatures.

The text in Lines 275-289 associated with Figure 3 has been revised as follows:

“ To further interpret the AHI-based diagnostics from a physical-space perspective, Figure 3 presents the time-averaged horizontal distributions of forecast-minus-observation (F–O) BT differences for AHI channel 13, together with OLR and CIWP simulated by WSM6 and NSSL.

Both simulations exhibit predominantly positive F–O differences over the equatorial region and near parts of the domain boundary, consistent with the more frequent occurrence of relatively warm channel-13 BTs (>270 K) compared with the observations in Figure 2. WSM6 shows more widespread positive F–O departures, which generally coincide with higher OLR and lower CIWP, suggesting a reduced amount of upper-level ice clouds. In contrast, NSSL exhibits generally smaller F–O biases, particularly over the 5–10° N region, although negative departures remain in some areas. Regions with reduced warm F–O biases in NSSL generally correspond to lower OLR and substantially larger CIWP. This spatial relationship is also consistent with the channel-13 BT frequency distributions in Figure 2, where NSSL exhibits a greater occurrence of cold BTs below approximately 230 K, suggesting a greater occurrence of cold upper-level ice clouds. A larger ice water path generally increases cloud optical thickness, shifting the effective emission level toward colder upper-cloud layers and thereby resulting in lower infrared window-channel brightness temperatures and reduced OLR (Marquis et al., 2023; Spang et al., 2024). The domain-averaged vertical hydrometeor profiles in Figure 8 provide further physical support by showing corresponding differences in upper-level frozen hydrometeor content between the two schemes.

References,

Marquis, J. W., Dolinar, E. K., Garnier, A., Campbell, J. R., Ruston, B. C., Yang, P., and Zhang, J.: Estimating the impact of assimilating cirrus cloud-contaminated hyperspectral infrared radiances for numerical weather prediction, *J. Atmos. Ocean. Tech.*, 40, 327–340, https://doi.org/10.1175/JTECH-D-21-0165.1, 2023.

Spang, R., Müller, R., and Rap, A.: Radiative effect of thin cirrus clouds in the extratropical lowermost stratosphere and tropopause region, *Atmos. Chem. Phys.*, 24, 1213–1230, https://doi.org/10.5194/acp-24-1213-2024, 2024.

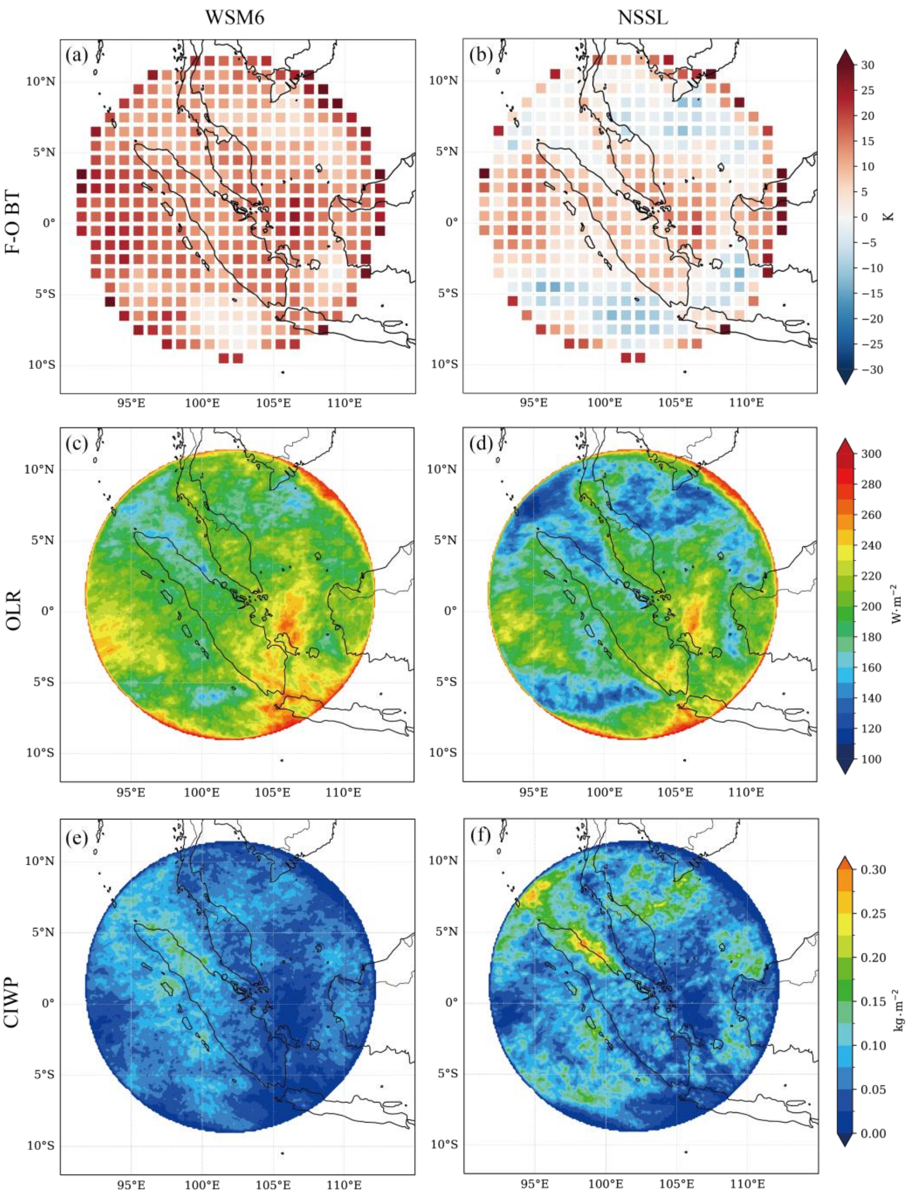

Figure 3. Daily-mean horizontal distributions of (a, b) AHI channel-13 forecast-minus-observation (F – O) brightness-temperature differences, (c, d) simulated outgoing longwave radiation (OLR), and (e, f) simulated cloud ice water path (CIWP) for WSM6

(left column) and NSSL (right column). Statistics are computed from 24-48 h forecasts at 6 h intervals using cloudy samples.

2) We also agree with the reviewer that the vertical hydrometeor distributions in Fig. 8 can help interpret several radiance-space features shown in Figs. 5 and 6, as discussed below. Compared with WSM6, NSSL exhibits a larger upper-tropospheric cloud fraction and greater cloud ice and snow contents between approximately 100 and 300 hPa. The uppermost level at which relative humidity reaches 100% is also generally higher in NSSL, indicating more extensive upper-level saturation conditions that favor the presence of high-level ice clouds. The greater amount of upper-level ice cloud in NSSL is consistent with the more frequent occurrence of low-CTP and cold-BT conditions in Fig. 6, reflecting a greater contribution from high, cold cloud tops. In contrast, the weaker upper-level cloud fraction and smaller cloud ice and snow contents in WSM6 are consistent with a greater occurrence of clouds with relatively higher CTPs and warmer BTs.

The vertical cloud structure in Fig. 8 also helps explain the cloud-type-dependent BT distributions in Fig. 5. For thick ice clouds, WSM6 substantially underpredicts the occurrence of cold BTs within approximately 200–240 K (Fig. 5). This behavior is consistent with the lower upper-level cloud-ice and snow contents and smaller cloud fraction shown in Fig. 8, suggesting a reduced occurrence of high, cold ice clouds. In addition, the pronounced overprediction of thin-ice-cloud cases below 240 K in NSSL (Figure 5) is consistent with the enhanced frozen hydrometeor content and larger cloud fraction above 200 hPa shown in Figure 8.

Following the reviewer's suggestion, we have revised several parts of the manuscript as follows:

"Lines 366-374: For optically thin ice clouds, WSM6 more accurately reproduces the observed frequency structure within the BT range of 220–290 K and BTDs of −2 to 5 K (Figures 5b and 5e). In contrast, NSSL overpredicts the occurrence of thin-ice-cloud cases with BTs below 230 K (Figures 5b and 5h). This higher occurrence of high-level ice-cloud cases is also reflected in the enhanced frozen hydrometeor content and larger cloud fraction above 200 hPa in NSSL (Figure 8). Despite these differences, both schemes show better performance for optically thin ice clouds than for the other ice-cloud regimes. Under thick-ice conditions, both simulations underpredict the observed frequencies (Figures 5c, f, and i), with WSM6 showing a larger bias than NSSL within the 200–220 K BT range. This relatively greater underprediction in WSM6 may be related to its lower upper-tropospheric cloud-ice and snow contents and reduced cloud fraction (Figure 8).

Lines 393-399: In both schemes, the simulated CTP frequencies are concentrated primarily between 100 and 200 hPa, with substantially fewer occurrences at 300–400 hPa than observed, indicating an overall bias toward higher cloud tops. For an infrared window channel, a higher cloud top generally shifts the effective emission level to colder atmospheric layers, resulting in a lower BT. The discrepancy is more pronounced in NSSL, which shows a higher frequency of cloud tops near 100 hPa and BTs below 220 K, consistent with its greater occurrence of thin ice clouds in the cold-BT regime (BTs < 220 K) relative to observations (Figures 5h and 5i). Meanwhile, the vertical hydrometeor distribution in NSSL shows enhanced frozen hydrometeor content and larger cloud fractions above 200 hPa (Figure 8). ”

3) Third, the simulated cloud microphysical characteristics are generally affected by model spin-up during the initial stage of the simulations. In general, the first 12 hours of the simulations should be excluded from the analysis. The authors should examine the temporal evolution of the cloud microphysical characteristics to ensure that the results are not significantly influenced by the spin-up process.

Reply: Thank you for this suggestion. To minimize the potential influence of model spin-up on our analysis, we have made several corresponding adjustments to the manuscript.

First, the diurnal-cycle analysis in Figure 7 has been revised to exclude the first 12 h of the simulations. The detailed revision is provided in our response to the following Comment 15).

We also examined the temporal evolution of the cloud microphysical characteristics shown in Figure 8. The differences between WSM6 and NSSL during the first 12 h are broadly consistent with those during the subsequent forecast period, suggesting that the main conclusions are not strongly influenced by the initial spin-up. In addition, most of the statistical analyses presented in the other figures are based on forecast samples after 24 h.

For Figure 4, we retain the full forecast period because the early evolution of cloud amount also provides useful information on the initial adjustment and the different rates of cloud development in the two simulations.

4) In addition, the choice of the cross-sections S0-2 for the analysis of the topographic clouds is unclear. Generally, the clouds are characterized in the normal direction to the Sumatora island. Please refer to Yokoi et al. (2017) and Okugawa et al. (2023).

Reply: Thank you for this helpful suggestion. We have revised the cross-section analysis accordingly. The revised cross-section locations are shown in Figure 1 below.

The original S0 cross-section has been removed from the manuscript. The S1 cross-section has been redefined to be oriented approximately normal to Sumatra Island, following Yokoi et al. (2017) and Okugawa et al. (2023). Figure 10 and the associated discussion have been revised accordingly, as detailed in our response to Comment 19).

We retain the S2 transect because it crosses a region where the two simulations show pronounced differences in the diurnal variation of F−O (Figure 9) and spans contrasting land and ocean environments. It therefore provides a complementary perspective on the relationships among cloud evolution, model differences, and land–sea contrasts. To clarify this purpose, the corresponding text in Lines 544-546 has been revised as follows:

"The S2 transect crosses a region where the two simulations exhibit distinct differences in the diurnal variation of F−O and spans the land-sea transition from the eastern Indian Ocean to western Java. The variations in near-surface temperature (T2 m) and specific humidity (Q2 m) along this transect further characterize the contrasting thermodynamic conditions (Figures 11a-b)."

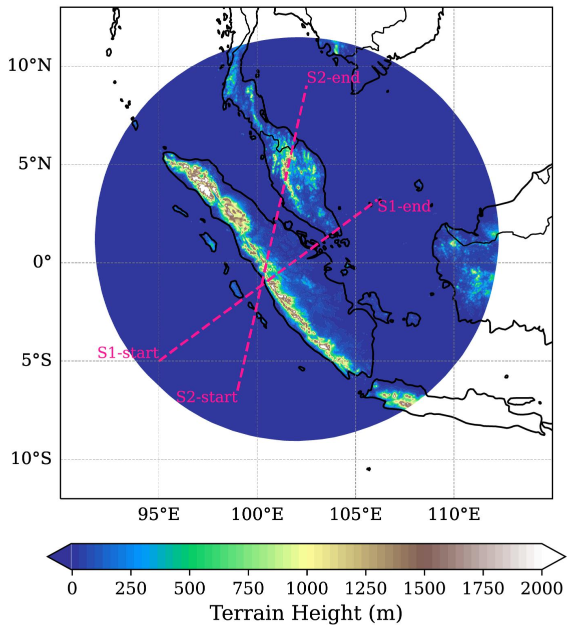

Figure 1. The terrain height (units: m) of MPAS simulation domain over the Maritime Continent, with three transects (S1–S2) used for subsequent cross-sectional analyses.

References:

Okugawa, R., K. Yasunaga, A. Hamada, and S. Yokoi, 2024: Numerical Study on the Precipitation Concentration over the Western Coast of Sumatra Island. *Mon. Wea. Rev.*, 152, 689–704,https://doi.org/10.1175/MWR-D-23-0037.1.

Yokoi, S., S. Mori, M. Katsumata, B. Geng, K. Yasunaga, F. Syamsudin, Nurhayati, and K. Yoneyama, 2017: Diurnal Cycle of Precipitation Observed in the Western Coastal Area of Sumatra Island: Offshore Preconditioning by Gravity Waves. *Mon. Wea. Rev.*, 145, 3745–3761,https://doi.org/10.1175/MWR-D-16-0468.1.

5) The most pronounced differences in brightness temperature between the two schemes appear to be associated with thin, high-level clouds. Such clouds are highly sensitive to the parameterization of cloud microphysical processes, and even small changes in model parameters can produce substantial changes in the simulated brightness temperatures. For example, the fall speed of cloud ice has often been adjusted to improve the simulated outgoing longwave radiation (OLR). However, the recently launched EarthCARE satellite now provides direct observations of cloud-ice fall speeds, offering a more physically based constraint for evaluating and improving cloud microphysics parameterizations. Therefore, the differences presented here may primarily reflect the sensitivity of high thin clouds to parameter tuning rather than fundamental differences between the two microphysics schemes.

Reply: Thank you for this insightful comment. Our evaluation indicates that simulated infrared brightness temperatures appear to be sensitive to the representation of high-level cloud ice. We agree that the pronounced BT differences for high-level thin ice clouds may be strongly influenced by sensitivities to microphysical parameter settings. At the same time, these sensitivities are not entirely independent of the underlying scheme formulations, which determine how particle size distributions, sedimentation, and ice-phase conversions are represented (Lim and Hong, 2010; Mansell et al., 2010). We therefore interpret the differences between WSM6 and NSSL as arising from the combined effects of their structural formulations and associated parameter settings, rather than attributing them solely to either factor.

Accordingly, the following discussion has been added to the Summary and Outlook section (Lines 617–621):

"The simulated BT differences between WSM6 and NSSL may reflect not only differences in their underlying microphysical formulations but also the strong sensitivity of cloud microphysical processes to parameter settings, particularly those governing upper-level ice clouds. Future work could additionally incorporate direct observations of cloud-ice fall speeds and vertical cloud structure from the EarthCARE satellite to provide more physically based constraints for evaluating and improving cloud microphysics parameterizations.”

Specific comments:

6) p. 8, Table 2, Channel 12: AHI cannot directly observe dynamic properties of the atmosphere. Potential vorticity is related to the Ozone distribution, but it is not adequate to be listed here.

Reply: Thank you for pointing this out. We have revised Table 2 by removing “potential vorticity” and listing Channel 12 (9.6 μm) as primarily sensitive to ozone.

7) L257-258: It is questionable whether fog is actually observed in this region. Is there any observational evidence?

Reply: Thanks for this comment. The two study periods were mainly characterized by convective cloud systems, and no clear or representative fog event was identified over the Singapore region. Moreover, nighttime channel-7 (3.9 μm) BTs alone cannot unambiguously distinguish surface fog from low-level clouds, as these features are typically identified using spectral differences with longwave infrared channels. The relevant sentences have therefore been revised more cautiously:

“Lines 251-252: Verification against nighttime channel 7 (3.9 μm) observations shows that NSSL more closely reproduces the observed cold-end BT distribution below 250 K.

Lines 266-269: A similar contrast is evident across several cloud-sensitive infrared channels, with WSM6 exhibiting a greater occurrence of relatively warm BTs and NSSL extending more prominently toward lower BTs. This contrast suggests that NSSL tends to produce more high-level, cold clouds, whereas the warmer BT distribution in WSM6 may reflect a greater contribution from lower, warmer clouds.”

8) L270-273: It is hard to draw the conclusion from the cross section shown by Fig. 3. The reviewer suggests showing the horizontal distribution.

Reply: Thank you for this suggestion. We have revised Fig. 3 accordingly by replacing the cross-sectional analysis with horizontal distributions. The revised results and corresponding discussion are presented in our response to previous Comment 1) and 2).

9) L281-283, "It is also noteworthy that the observed cloud-top heights are lower than those simulated by both schemes. Such discrepancies likely stem from excessive condensate lofting through enhanced updrafts": Higher cloud top is generally associated with too strong intensity (vertical draft or precipitation) of convection. If excessive condensation is due to strong precipitation, this interpretation is incorrect.

Reply: Thank you for this clarification. We agree that our previous interpretation could be misleading. The corresponding statement and cross-sectional figure have been removed from the revised manuscript and replaced with horizontal distributions.

10) L371-372: By comparing Fig. 5c with Fig 5f,i, we do not think WSM6 is particularly underpredicted. Both WSM6 and NSSL shows underpredecition of frequencies than the observation.

Reply: Thank you for this comment. We agree that both WSM6 and NSSL underpredict the observed frequencies under thick-ice conditions. We also note that WSM6 shows a larger bias than NSSL within the 200−220 K BT range. The text in Lines 371-372 has therefore been revised to more accurately characterize the differences between the two simulations, as follows:

" Under thick-ice conditions, both simulations underpredict the observed frequencies (Figures 5c, f, and i), with WSM6 showing a larger bias than NSSL within the 200–220 K BT range. "

11) L383: What is the definition of cloud-top here in the observation? Is ECMWF IFS data used for the observational analysis?

Reply: Thank you for this comment. The observed cloud-top height is obtained from the Himawari-9 AHI Level-2 cloud-height product and represents a radiatively retrieved cloud-top height derived from multispectral infrared observations. ECMWF IFS data are not used in the observational analysis. The corresponding description has been added in Lines 386–387, as follows:

" The observed cloud-top height is obtained from the Himawari-9 AHI Level-2 cloud-height product and represents a radiatively retrieved cloud-top height derived from multispectral infrared observations. "

12) L391-400: It is difficult to understand the description here. Are the biases of too-high CTP due to high thin clouds being overestimated in the simulations? The difference in the PDF of BT of Channel 13 is shown in Fig. 2. Both models show too much warmer BT frequency. However, Fig. 6 shows most CTP are near 100-200 hPa. The question is what the cloud structure representing AHICH13 BT > 280 K?

Reply: Thank you for pointing out this ambiguity.

1) Regarding the first question, Figure 6 shows that both simulations produce cloud tops predominantly between 100 and 200 hPa, while underrepresenting cloud tops between 250 and 600 hPa relative to the observations. This indicates an overall tendency for the simulated cloud tops to be too high. The cloud-type distributions in Figure 5 may provide a possible explanation for this bias. Both simulations exhibit an increased occurrence of thin ice clouds in the cold-BT regime compared with the observations, with this feature being more pronounced in NSSL. Consistently, NSSL also produces greater frozen-hydrometeor content and larger cloud fractions above 200 hPa (Figure 8), together with a notably higher frequency of cloud tops around100 hPa than both the observations and WSM6 (Figure 6). These results suggest that the excessive occurrence of high cloud tops may be partly associated with an overrepresentation of high-level thin ice clouds, particularly in NSSL. The tendency toward excessively high cloud tops in both schemes may also be partly related to the 3-km grid spacing. Kilometer-scale simulations can produce larger convective cells with weaker entrainment of midlevel environmental air, thereby favoring deeper convection and higher cloud tops (Bryan and Morrison, 2012).

To clarify the description and address this concern, the corresponding sentences have been revised as follows:

"Lines 393-399: In both schemes, the simulated CTP frequencies are concentrated primarily between 100 and 200 hPa, with substantially fewer occurrences at 300–400 hPa than observed, indicating an overall bias toward higher cloud tops. For an infrared window channel, a higher cloud top generally shifts the effective emission level to colder atmospheric layers, resulting in a lower BT. The discrepancy is more pronounced in NSSL, which shows a higher frequency of cloud tops near 100 hPa and BTs below 220 K, consistent with its greater occurrence of thin ice clouds in the cold-BT regime (BTs < 220 K) relative to observations (Figures 5h and 5i). Meanwhile, the vertical hydrometeor distribution in NSSL shows enhanced frozen hydrometeor content and larger cloud fractions above 200 hPa (Figure 8).

Lines 594-596: The cloud-top biases may also be partly related to the 3-km grid spacing, as relatively coarse kilometer-scale grids can produce larger convective cells with reduced entrainment of midlevel environmental air, thereby favoring higher cloud tops (Bryan and Morrison, 2012). "

2）Regarding channel-13 BTs above 280 K, AHI channel 13 (10.4 µm) is an infrared window channel. Under cloudy conditions, relatively warm BTs can arise from low-level warm clouds or semitransparent high clouds, for which thermal emission from warmer underlying cloud layers and/or the surface can partially transmit through the cloud and contribute to the top-of-atmosphere radiance (Marchand et al., 2010; Wang et al., 2013). This interpretation is also supported in some regions by the lower cloud ice water path (CIWP) and higher outgoing longwave radiation (OLR) shown in Figure 3, suggesting weaker cloud infrared opacity. In addition, uncertainties in cloud detection and cloud-sample selection in the AHI Level-2 product may also affect the warm-BT distribution.

The related sentences have been revised as follows (Lines 261-266):

" Moreover, both microphysics schemes exhibit a higher frequency of warm BTs around 280-295 K than observed. These warm BTs may be associated with semitransparent high-level clouds, consistent in some regions with the lower cloud ice water path (CIWP) and higher outgoing longwave radiation (OLR) shown in Figure 3. For such clouds, thermal emission from warmer underlying cloud layers and/or the surface can partially transmit through the cloud and contribute to the top-of-atmosphere radiance (Marchand et al., 2010; Wang et al., 2013). In addition, uncertainties in the AHI Level-2 cloud detection may also affect the warm -BT distribution. "

References,

Bryan, G. H. and Morrison, H.: Sensitivity of a simulated squall line to horizontal resolution and parameterization of microphysics, *Mon. Weather Rev.*, 140, 202–225, https://doi.org/10.1175/MWR-D-11-00046.1, 2012.

Marchand, R., Ackerman, T., Smyth, M., and Rossow, W. B.: A review of cloud top height and optical depth histograms from MISR, ISCCP, and MODIS, *J. Geophys. Res. Atmos.*, 115, D16206, https://doi.org/10.1029/2009JD013422, 2010.

Wang, C., Yang, P., Platnick, S., Heidinger, A. K., Baum, B. A., Greenwald, T., Zhang, Z., and Holz, R. E.: Retrieval of ice cloud properties from AIRS and MODIS observations based on a fast high-spectral-resolution radiative transfer model, *J. Appl. Meteor. Climatol.*, 52, 710–726, https://doi.org/10.1175/JAMC-D-12-020.1, 2013.

13) L414: "5g" should be "5h".

Reply: Corrected.

14) L418, "multilayered ice clouds": What is the definition of multilayered clouds?

Reply: Thank you for this comment. In this study, "multilayered ice cloud" refers to a predefined cloud-type category in the AHI Level-2 cloud product, representing a semitransparent upper-level ice cloud overlying an opaque lower cloud layer. We have revised the sentences in Lines 423-424 to clarify this definition as follows:

“ Multilayered ice clouds are defined here as semitransparent upper-level ice clouds overlapping a lower opaque cloud layer (Pavolonis and Calvert, 2020). ”

References,

Pavolonis, M., and Calvert, C.: NOAA Enterprise cloud type and cloud phase, version 3, Algorithm Theoretical Basis Document, NOAA NESDIS Center for Satellite Applications and Research, 106 pp., https://www.star.nesdis.noaa.gov/goesr/documents/ATBDs/Enterprise/ATBD_Enterprise_Cloud_Type_v3_2020-06-01.pdf, 2020.

15) L422-429: The reviewer does not find the analysis presented in Fig. 7 to be particularly informative. It is difficult to identify the differences between the two microphysics schemes. The effects of model spin-up in the first half a day would have also affected the results. The authors should reconsider their approach and adopt a more robust method for illustrating the differences in the simulated diurnal variations and their biases relative to the observations.

As a first step, the reviewer recommends analyzing the two most fundamental characteristics of the diurnal cycle: its phase and amplitude in BR of Channel 13. A comparison of these quantities between the observations and the simulations would provide a clearer and more quantitative assessment of model performance.

Reply: Thank you for this constructive suggestion. Following the reviewer’s recommendation, Figure 7 has been revised to provide a more quantitative characterization of the diurnal evolution of the Channel-13 F–O differences. In particular, the diurnal amplitude is quantified using a first-harmonic analysis, while the timing of the diurnal variation is further characterized in the corresponding discussion. To minimize the influence of model spin-up on these quantitative diagnostics, the first 12 h of each forecast are excluded from the revised analysis. These revisions allow the magnitude of the F – O biases and their diurnal characteristics to be more clearly assessed between the two microphysics schemes. The corresponding text in the first two paragraphs of Section 3.3, together with Figure 7, has been revised as follows:

“ Figure 7 displays the probability distributions of channel 13 F–O BTs as a function of forecast lead time for the WSM6 and NSSL schemes under different cloud-type conditions. To minimize the influence of model spin-up on the quantitative assessment, the first 12 h of each forecast are excluded from the analysis. The amplitude of the diurnal variation is quantified using a first-harmonic fit with a 24-h period applied to the median F–O evolution over the 12–36 h forecast period. For liquid-water clouds (5–6 % of total cloud samples), both schemes show relatively good consistency between simulated and observed BTs. The corresponding F–O distributions are tightly centered around zero and exhibit minimal temporal variability (Figures 7a-b). For optically thin ice clouds, representing about 45% of the total samples, this category is predicted most accurately by both schemes among all ice-cloud types. This behavior is characterized by smaller F–O biases and lower standard deviations (STDs), particularly in WSM6 (Figures 7c-d). The better performance of WSM6 for optically thin ice clouds is also consistent with Figure 5, where WSM6 more closely reproduces the observed cloud-type frequency than NSSL. Under optically thick ice cloud conditions (Figures 7e–f), the contrast between the two schemes becomes more pronounced. NSSL performs substantially better, with a much smaller mean warm bias of 4.8 K compared with 26.3 K for WSM6. The larger warm bias in WSM6 (Figure 7e) is in line with its underprediction of optically thick ice cloud frequency in the cold-BT regime (Figures 5c and 5f). This behavior is further reflected in the vertical hydrometeor distributions in Figure 8, which show substantially lower upper-tropospheric cloud-ice and snow contents in WSM6 than in NSSL. Multilayered ice clouds are defined here as semitransparent upper-level ice clouds overlapping a lower opaque cloud layer (Pavolonis and Calvert, 2020). They account for 25.7% of the total cloud samples and show the lowest simulation skill in both schemes, as evidenced by broad probability plumes displaced from 0 K and the largest STDs among all cloud categories (Figures 7g-h).

The pronounced diurnal variations in F–O are evident under optically thick and multilayered ice-cloud conditions. For optically thick ice clouds, both schemes exhibit a comparable diurnal evolution, with F–O decreasing from 20:00 to 08:00 SGT and increasing thereafter toward 20:00 SGT; the corresponding amplitudes are 4.0 K for WSM6 and 2.9 K for NSSL. In contrast, the two schemes show clearly different diurnal behavior for multilayered ice clouds, with amplitudes of only 0.9 K in WSM6 but 23.5 K in NSSL. In NSSL, F–O decreases markedly from 02:00 to 14:00 SGT, followed by an increase toward nighttime. An approximately 6-h phase difference is evident between the diurnal variations of optically thick and multilayered ice clouds in NSSL. The physical-space characteristics associated with these diurnal variations are further examined in the following sections. ”

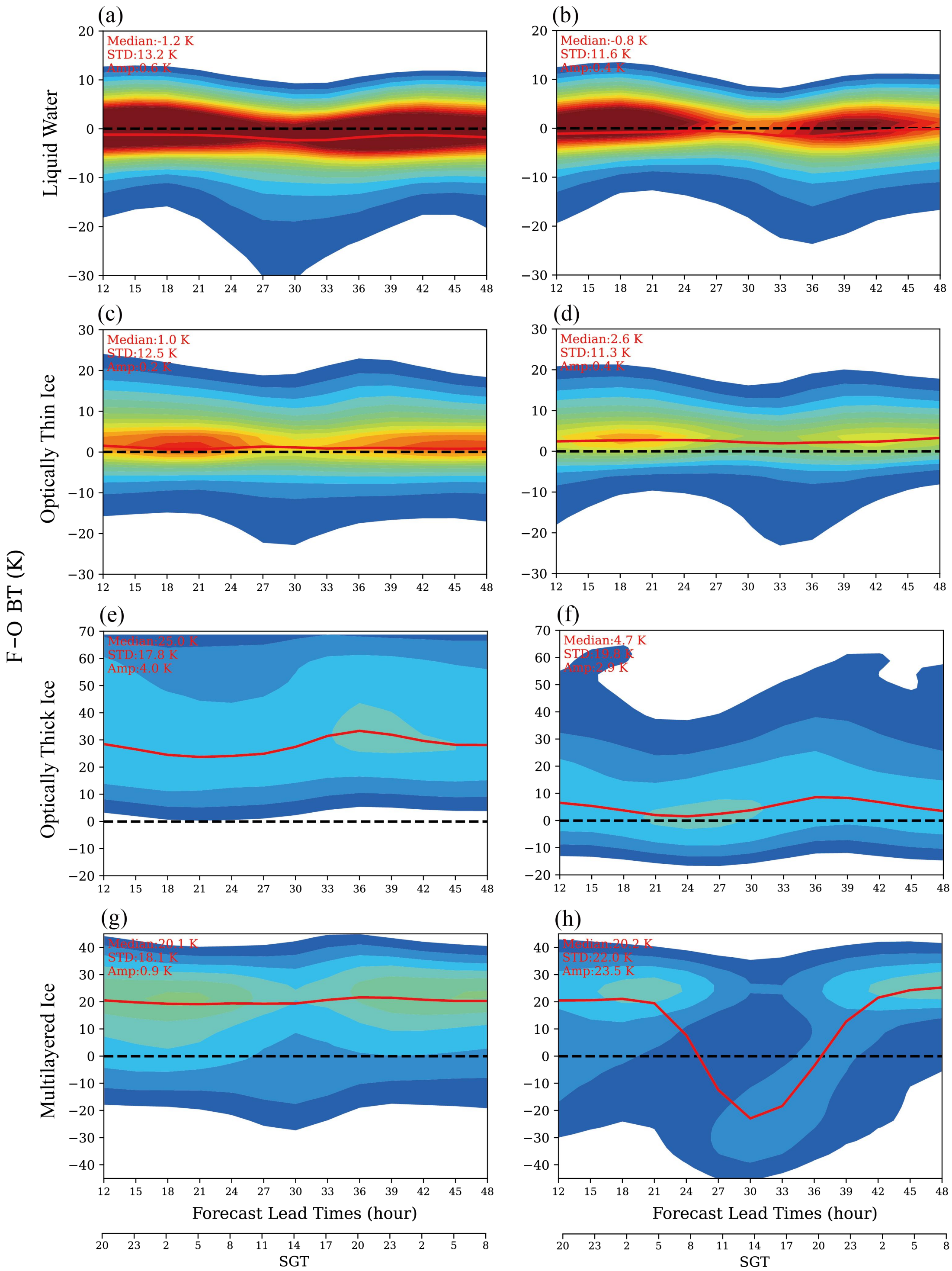

Figure 7. Probability distributions of channel 13 Forecast-Minus-Observation brightness temperature (F−O BT; units: K) as a function of forecast lead time (from 00:00 UTC) for WSM6 (first column) and NSSL (second column) under four cloud-type conditions. Lead time-averaged median, standard deviation and amplitude of F−O are shown in each legend. The red line denotes the median values at different forecast ranges.

16) p. 22-24, Figure 8: This figure clearly demonstrates the differences in the cloud microphysical characteristics simulated by the two schemes. In particular, thin, high-level clouds are much more abundant in the NSSL scheme than in WSM6. How do these differences in high thin cloud coverage affect the results shown in Figs. 5 and 6?

Reply: Thank you for this suggestion. In Figure 5h, NSSL exhibits a markedly higher frequency of scenes classified as thin ice in the cold-BT regime (<230 K) than both the observations and WSM6, indicating a more frequent occurrence of high-level thin-ice clouds. Consistently, Figure 6c shows that NSSL has a pronounced concentration of cloud tops near 100 hPa within the same cold-BT range, with frequencies exceeding those in both the observations and WSM6. Taken together, the enhanced occurrence of cold thin-ice scenes in Figure 5 and the shift toward very low CTPs in Figure 6 are consistent with the more abundant high-level thin ice clouds simulated by NSSL in Figure 8.

The corresponding discussion in Lines 461–469 of the revised manuscript has been revised as follows:

" In contrast to WSM6, the saturation layer in NSSL is positioned at a higher altitude (~250 hPa), accompanied by enhanced concentrations of Qi (~0.034 g kg^{-1}) and Qs (~0.078 g kg^{-1}) extending through the 350–150 hPa layer (Figures 8b and 8d). This tendency is consistent with previous MPAS- and WRF-based evaluations showing larger cloud-ice mixing ratios in NSSL than in WSM6 (Chen et al., 2026; Morrison et al., 2015). The enhanced ice condensate may partly contribute to the smaller F–O biases for optically thick ice clouds in NSSL, whereas a relatively large positive bias persists for optically thin ice-cloud scenes (Figures 7d and 7f). Moreover, the greater abundance of high-level thin ice clouds in NSSL shown in Figure 8b is closely associated with substantially higher frequencies of thin-ice scenes at cold BTs below ~240 K (Figure 5h) and a higher frequency of cold-cloud tops near 100 hPa than observed (Figure 6c). "

17) The authors attempt to explain the underlying mechanism based on these results (pp. 23– 24). However, the analysis presented is primarily diagnostic of relationships. It does not establish the physical mechanisms or causes responsible for the biases in the simulated diurnal variability. The authors should reconsider this section, ensuring that the conclusions are better supported by the results presented.

Reply: The discussion in this section has been revised to better reflect the scope of the analyses presented. The current diagnostics primarily characterize the relationships between the Channel-13 F-O variations and the simulated cloud and hydrometeor fields, rather than establishing direct causal mechanisms. Accordingly, the corresponding text has been revised to avoid causal interpretations that are not explicitly supported by the results, as follows:

“1) Lines 433-434: The physical-space characteristics associated with these diurnal variations are further examined in the following sections.

2)Lines 470-482: The stronger diurnal variability of F–O in NSSL under multilayered ice-cloud conditions (Figure 7) coincides with larger diurnal variations in upper-tropospheric ice-phase hydrometeors (Qi and Qs) between approximately 300 and 100 hPa (Figures 8b and 8d). During the daytime convective period (14:00–17:00 SGT), enhanced upper-level cloudiness and larger Qi and Qs in NSSL are associated with colder simulated BTs and more negative F–O values (Figure 7h). In contrast, the nighttime reduction in ice-phase hydrometeor contents is accompanied by a shift toward more positive F–O values (Figures 7h, 8b, and 8d). For optically thick ice clouds, however, WSM6 exhibits a relatively large diurnal amplitude of F–O than NSSL (Figure 7e). This variation appears to be associated with larger diurnal changes in Qc and Qg, with higher hydrometeor contents during 23:00–05:00 SGT corresponding to reduced positive F–O biases, whereas lower hydrometeor contents during 17:00–23:00 SGT coincide with increased positive biases (Figures 8a and 8c). Furthermore, the larger variations in F–O bias with broader, lower-frequency distributions during 11:00–17:00 SGT appear to be associated with enhanced hydrometeor contents, suggesting more active cloud microphysical evolution during the daytime. In contrast, the nighttime period of 20:00–05:00 SGT is characterized by weaker F–O variability and more persistent high-frequency distributions, together with generally reduced hydrometeor contents and potentially weaker cloud microphysical activity.”

18) p. 27, Figure 10: What is the meaning of “Mean cross-section”? Is it the same as the domain average?

Reply: “Mean cross-section” refers to the temporal average of vertical cross-sections along the same prescribed transect over the selected forecast hours, rather than a domain average. To clarify this, we have revised the figure caption and corresponding text accordingly:

“Lines505-508: Figures 10-11 present daytime- and nighttime-averaged cross-sections of simulated cloud fraction, vertical velocity, and thermodynamic fields along the S1 and S2 transects shown in Figure 1. The averages are calculated from forecast samples within the corresponding daytime (11:00–17:00 SGT) and nighttime (21:00–03:00 SGT) periods.

Lines539-543: Figure 10. Daytime- and nighttime-averaged cross-sections of the cloud fraction (blue-filled contours), vertical velocity (black vectors; units: m/s), equivalent potential temperature anomaly (red contours; units: K), minimum observed cloud-top pressures (purple lines; units: hPa) and terrain height (grey shading; units: km) along the S1 transect shown in Figure 1 for the (a, b) 11:00-17:00 SGT daytime from a forecast range of 3-9 h and 27-33 h and (c, d) 21:00-03:00 SGT nighttime from the 13-19 h and 37-43 h forecasts in WSM6 (first column) and NSSL (second column) experiments.

19) p. 25, Figures 10 and 11: It is difficult to gain insight into the general characteristics of convection over the topography from these figures. In particular, it is unclear what additional information Fig. 10, which is shown along the line S1 parallel to the mountain range, provides.

Instead, the authors are encouraged to analyze a cross section taken normal to the Sumatra mountain range (normal to S1). This would provide a much clearer representation of the general convective structure and its relationship to the topography.

Reply: Thank you for this helpful suggestion. Following the reviewer's suggestion, we have revised the orientation of the cross section to be approximately normal to the local orientation of the Barisan Mountain range, consistent with the approaches adopted by Yokoi et al. (2017) and Okugawa et al. (2024). Figure 10 and the corresponding discussion have been revised accordingly, and the rationale for selecting this transect has been clarified in the revised manuscript as follows:

" To further examine the influence of topography and atmospheric environments on cloud diurnal evolution, Figures 10-11 present daytime- and nighttime-averaged cross-sections of simulated cloud fraction, vertical velocity, and thermodynamic fields along the S1 and S2 transects shown in Figure 1. The averages are calculated from forecast samples within the corresponding daytime (11:00–17:00 SGT) and nighttime (21:00–03:00 SGT) periods.

Following Yokoi et al. (2017) and Okugawa et al. (2024), the S1 cross section shown in Figure 10 spans different terrain types and is oriented approximately normal to the Sumatra mountain range (Barisan Mountains), where the terrain rises to elevations of approximately 1 km. During the daytime, both schemes exhibit enhanced positive potential temperature anomalies around the elevated terrain, accompanied by strong vertical motions and extensive cloud coverage between 400 and 100 hPa (Figures 10a-b). This pronounced convective development over the mountainous region is consistent with Okugawa et al. (2024), who suggested that daytime solar heating, land-sea circulation, and orographic forcing may favor vigorous convection over Sumatra land, particularly promoting upper-level ice-cloud development. These daytime characteristics also help explain the larger negative F–O biases over land (Figures 9a-b), as enhanced high-level cloud coverage over the Barisan Range raises the effective infrared emission level to colder atmospheric layers, resulting in lower simulated BTs. Compared with WSM6, NSSL exhibits deeper convective updrafts over the mountain near 100° E, with enhanced vertical motion extending to higher levels and accompanied by greater upper-level cloud fraction (>0.7 above ~300 hPa). The greater amount of high-level clouds over the mountainous terrain are consistent with the larger negative F – O biases in Figure 9b. In contrast, over the low-elevation marine regions, negative potential temperature anomalies are accompanied by relatively weak updrafts and reduced upper-level cloud development (Figures 10a-b), consistent with the positive F – O biases in both schemes (Figures 9a-b). The weaker upper-tropospheric ascent in WSM6 compared with NSSL may be partly related to its enhanced graupel content shown in Figure 8, as increased hydrometeor loading can reduce net buoyancy and thereby suppress updraft development (Conrick et al., 2018). It is also noteworthy that NSSL produces greater upper-tropospheric cloud coverage than WSM6 over both land and ocean, consistent with the larger amounts of high-level ice-phase hydrometeors shown in Figure 8.

After sunset, the thermodynamic and cloud structures over the adjacent seas show relatively weak diurnal variations, consistent with the small day-night differences in F–O biases. Over the mountainous region (~100°–103° E), however, the cross-sectional structure exhibits pronounced diurnal differences. Specifically, both schemes exhibit larger positive F –O biases over the mountainous region (Figures 9c–d), coinciding with weaker upward motion and reduced upper-level cloud amount at night (Figures 10c–d). Notably, the larger nighttime positive bias in WSM6 is consistent with the scarcity of cloud cover above 300 hPa (Figure 10c). The pronounced day–night contrast over the mountainous terrain may be attributed to the terrain-modulated diurnal cycle of surface heating and local circulation. During the daytime, enhanced solar heating over elevated terrain can strengthen upslope flow and convective instability, thereby promoting cloud development (Hartmann et al., 2018; Pepin et al., 2022). At night, radiative cooling stabilizes the lower atmosphere and weakens thermally driven upslope circulation, resulting in reduced vertical motion and suppressed convective cloud development over the mountains (Sokol et al., 2020). ”

References,

Okugawa, R., Yasunaga, K., Hamada, A., and Yokoi, S.: Numerical study on the precipitation concentration over the western coast of Sumatra Island, *Mon. Weather Rev.*, 152, 689–704, https://doi.org/10.1175/MWR-D-23-0037.1, 2024.

Yokoi, S., Mori, S., Katsumata, M., Geng, B., Yasunaga, K., Syamsudin, F., Nurhayati, N., and Yoneyama, K.: Diurnal cycle of precipitation observed in the western coastal area of Sumatra Island: Offshore preconditioning by gravity waves, *Mon. Weather Rev.*, 145, 3745–3761, https://doi.org/10.1175/MWR-D-16-0468.1, 2017.

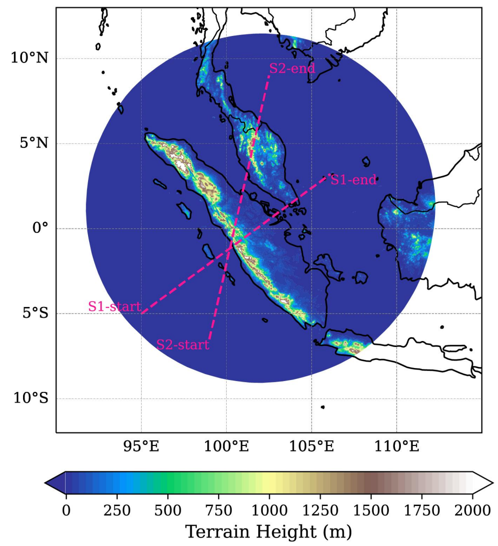

Figure 1. The terrain height (units: m) of MPAS simulation domain over the Maritime Continent, with three transects (S1 – S2) used for subsequent cross-sectional analyses.

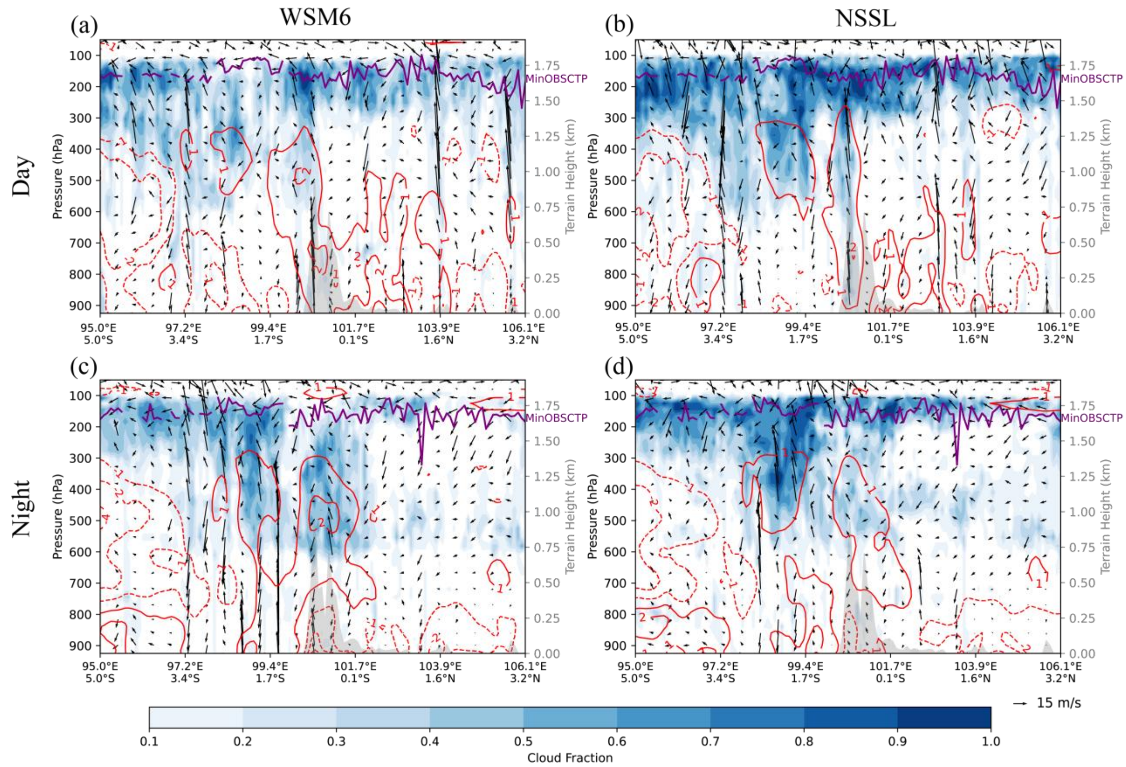

Figure 10. Daytime- and nighttime-averaged cross-sections of the cloud fraction (blue-filled contours), vertical velocity (black vectors; units: m/s), equivalent potential temperature anomaly (red contours; units: K), minimum observed cloud-top pressures (purple lines; units: hPa) and terrain height (grey shading; units: km) along the S1 transect shown in Figure 1 for the (a, b) 11:00-17:00 SGT daytime from a forecast range of 3-9 h and 27-33 h and (c, d) 21:00-03:00 SGT nighttime from the 13-19 h and 37-43 h forecasts in WSM6 (first column) and NSSL (second column) experiments.